International Forum on Aeroelasticity and Structural Dynamics
IFASD 2024
17 – 21 June 2024, The Hague, The Netherlands

AEROELASTIC WIND TUNNEL TESTING OF 3D-PRINTED SEMISPAN WINGS

Alexander M. Pankonien[1], Nicholas Jones[2], Asa Palmer[3], Joshua Deslich[1], Kevin McHugh[1], and Robert Taylor[4]

[1]U.S. Air Force Research Laboratory, Wright-Patterson Air Force Base, Ohio, USA, alexander.pankonien.1@us.af.mil, joshua.deslich.1@us.af.mil, kevin.mchugh.3@us.af.mil

[2]PCKrause & Associates, Dayton, Ohio, USA, njones@pcka.com

[3]University of Dayton Research Institute, Dayton, Ohio, USA, asa.palmer@udri.udayton.edu

[4]University of Texas Arlington, Arlington, TX, USA, taylorrm@uta.edu

Additive manufacturing has lowered barriers associated with rapidly realizing complex shapes, such as the airfoils of wind tunnel models. To construct a flexible, aeroelastic wind tunnel model, these printed airfoils are typically affixed to an underlying structure, made with conventional fabrication techniques. However, the resultant design is not representative of the topologies typically found in aircraft, complicating actuation and sensing integration. This work details several years of exploring aeroelastic wind tunnels that leverage new, printed materials to build the underlying load bearing structure and skins. It is hoped that building all load bearing components simultaneously will reduce integration complexity, as well as lower overall fabrication cost and time, providing an opportunity for data assimilation into a conceptual vehicle design process. The method employed to design these models is a traditional conceptual aircraft sizing tool that allocates material thickness, and material stiffness when applicable to the printing process. This technique has been demonstrated for statically and dynamically scaled 20-inch semi-span models of a flying wing. Models in this work have been fabricated using one of two printing processes for comparison—polyjet or selective laser sintering. The models have been structurally tested experimentally, both quasi-statically and dynamically to validate their properties. The quasi-static deflection of the models under aerodynamic loading has been measured via digital image correlation measurement during wind tunnel testing, showing good agreement with expected stiffness, albeit with creep in the polyjet models. Initial efforts using the same experimental setup to characterize dynamic aeroelastic characteristics are also described, indicating the need for external excitation in these more highly-damped material systems. Finally, initial scanning of airfoil measurement for data assimilation is described, indicating good outer mold line agreement with the as-designed geometries in camber, but up to two degrees of erroneous twist. These results show promise for even larger models made with selective laser sintering of materials with higher glass transition temperatures.

1 INTRODUCTION

Aeroelastic wind tunnel models have traditionally been manufactured using a beam and follower shell approach [1]. Here the stiffness of the full scale vehicle is "condensed" to a idealized Euler-Bernouli beam about the elastic axis of the wing with followers giving the aerodynamic shape. The followers ideally do not contribute to the stiffness of the model, but simply communicate the aerodynamic forces from the flow to the beam. The cross sectional stiffness properties of this beam, the bending stiffness EI and the torsional stiffness GJ, are scaled continuously over

the span of the wing, from the full-scale vehicle to the sub-scale size using scaling laws [2]. For the same flow conditions, i.e. freestream flow speed and Mach Number, this scaling factor is simply the geometric scale factor:

$$\Lambda_G = G_{FS}/G_{SS} \tag{1}$$

It then is up to the designer of the wind tunnel model to interpret which materials and cross sectional geometry will give the appropriate cross sectional stiffness properties. With this step accomplished, the designer can then simply add nonstructural masses to tailor the dynamic responses to create both a statically and dynamically scaled model.

However, achieving appropriate cross sectional properties is often more challenging due to practical manufacturing constraints. Specifically, aerospace structures are often weight-constrained, and thus constructed of stiff, strong materials used in thin shell elements. To accomplish the design of a subscale model from a full scale design, ideally one would reduce the thickness of all elements while maintaining the same material properties. However, maintaining the use of similar stiffness materials to that of the full scale vehicle would necessitate even thinner structures. Because the original structures were already thin, the resultant subscale designs quickly become constrained by either machining tolerances or minimal ply thicknesses. Further challenges are then posed by attachments to these thin structural members, such as nonstructural masses and follower shells for passive models, and also control surfaces, actuators, and sensors for active models. Even if these challenges can be practically overcome, they result in either very high manufacturing costs or problematic handling requirements.

These constraints drive compromises in the resultant subscale design and can potentially be addressed by alternative designs or manufacturing techniques. The first known use of multi-material additive manufacturing to create a dynamic aeroelastic wind tunnel model was Pankonien & Reich in 2017 [3]. This model used an ad-hoc sized conventional rib and spar internal topology where only structural material properties were replaced by photopolymer thermoplastics to achieve the requisite material stiffness. Since then, work to use metal additive manufacturing with hollow internal structure for transonic aeroelastic wind tunnel models has also progressed [4]. There has also been mixed used of additive manufacturing with conventional monokote skin and carbon fiber spars to create active aeroelastic wind tunnel models [5].

The use of topology optimization has led to replacing the underlying structure, also known as the inner mold line, with nonconventional layouts in pursuit of the appropriate mass and stiffness distributions for dynamic scaling, such as found in Stanford [6]. However the realization of complex layouts has been found to be subject to manufacturing constraints, especially at a small scale, and material properties insufficiences as softer materials are used. These choices have driven the interpretation of optimized topologies [7] to either be thin flat plates or curvilinear spars and ribs [8].

1.1 Scope and Contribution of Current Work

The current work focuses on an aeroelastic wind tunnel test campaign as part of a risk reduction effort to more rapidly and affordably obtain experimental data from multiple aircraft configurations generated by an in-house conceptual aircraft design process. The effort was conducted at the Air Force Research Laboratory at Wright-Patterson Air Force Base in Dayton, Ohio. The name of the program was Aeroelastic Wind tunnel Experimental Capability to Support MDAO (i.e. AWECSM), see Figure 1. The end goal of the program would be to provide relevant experimental data on a timescale commensurate with model design closure.

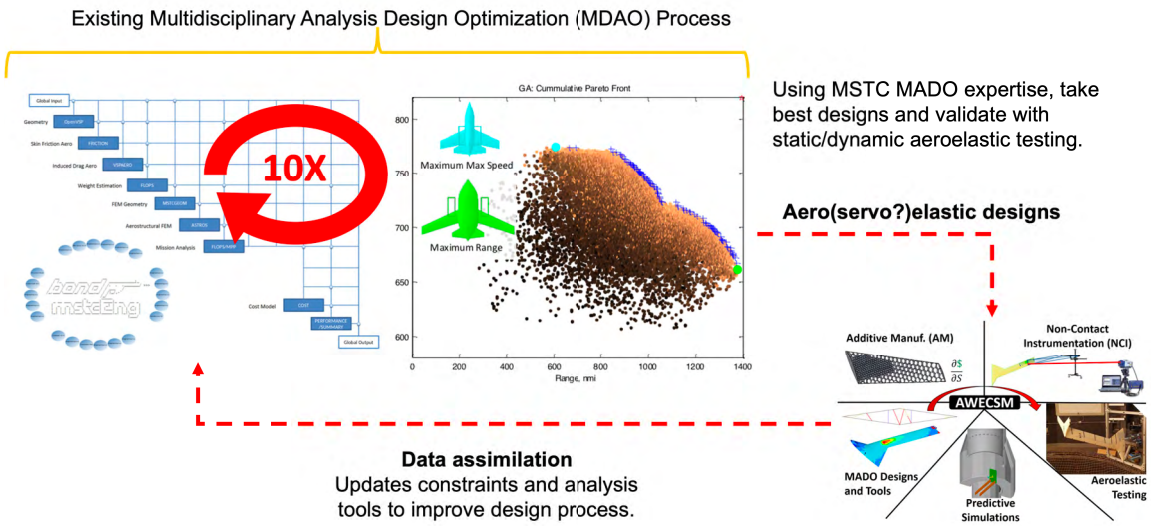

Figure 1: Linking MDAO aircraft design with an experimental aeroelastic capability

The program's primary emphasis focused on how 3D-printing could accelerate aeroelastic wind tunnel testing. Following the literature review above, the primary scientific contribution of the work was to understand the challenges and possibilities associated with using polymeric primary structure in the creation of scaled aeroelastic wind tunnel models.

Prior work by the authors have discussed the process for utilizing sizing optimization to perform quasi-static aeroelastic scaling of completely 3D-printed polymer models [9]. Subsequent efforts included experimental validation of the stiffness of 3D-printed models using such methods [10].

Pushing towards the goal of rapid static and dynamically scaled aeroelastic models, this work will detail the dynamic structural testing, as well as quasi-static aeroelastic wind tunnel testing, dynamic aeroelastic wind tunnel testing, and geometry inspection of the designs created by the method established in prior work.

2 WIND TUNNEL TESTING

There were multiple goals for the wind tunnel test to prove the viability of rapid, low-cost aeroelastic wind tunnel testing for design validation at the Air Force Research Laboratory. Achieving these goals would serve as a risk reduction for future efforts to incorporate data assimilation from experimental testing into the conceptual aircraft design process. The goals were articulated in discussions with other AFRL researchers as to 1) bring more models linked to a conceptual aircraft design process to the wind tunnel test at the same time, 2) to identify repeatable metrics for those models along with relevant uncertainty metrics, and 3) any sort of dynamic aeroelastic measurement, in addition to quasi-static measurement.

The metrics of performance identified related to these goals were then 1) measuring "compliance" of the models at different flow speeds, 2a) the number of designs brought to a single wind tunnel test, and 2b) re-printing multiple instances of the same design for repeat testing at the same flow condition, and 3) frequency response of model vibraition in the wind tunnel due to ambient excitation. The following sections detail how these measure of performance were achieved.

2.1 Wind tunnel description

The aeroelastic models were tested in the new Subsonic Research Facility (i.e. SuRF) [11], which was constructed purposefully for the testing of subsonic wind tunnel models with lower safety factors than traditional models, allowing test-to-failure. The SuRF operates in a continuous flow, closed jet, subsonic blow down configuration. There are three test sections, each 4 foot (1.219 m) cubes that are arrayed sequentially. Installation of a model in the last test section then permits test of models to failure due to lack of critical instrumentation or rotating machinery downstream of this section.

2.2 Experimental Setup Description

A custom splitter plate constructed of medium density fiberboard was installed to move the symmetry plane of the models 4.75 inches (12 cm) above the floor in the third test section to ensure the models would be clear of the growing boundary layer in this section, shown in Figure 2 A circular hole in the splitter plate allowed a fixed base connected to an external rotary table to rotate the semi-span models freely 360 degrees about their pitch axis under aerodynamic load. With this setup, the speed controller for the SuRF offered closed-loop control over freestream flow speeds from approximately 10 m/s to greater than 30 m/s, although, due to safety factor calculations for the splitter plate, the speed within the tunnel did not exceed 30 m/s.

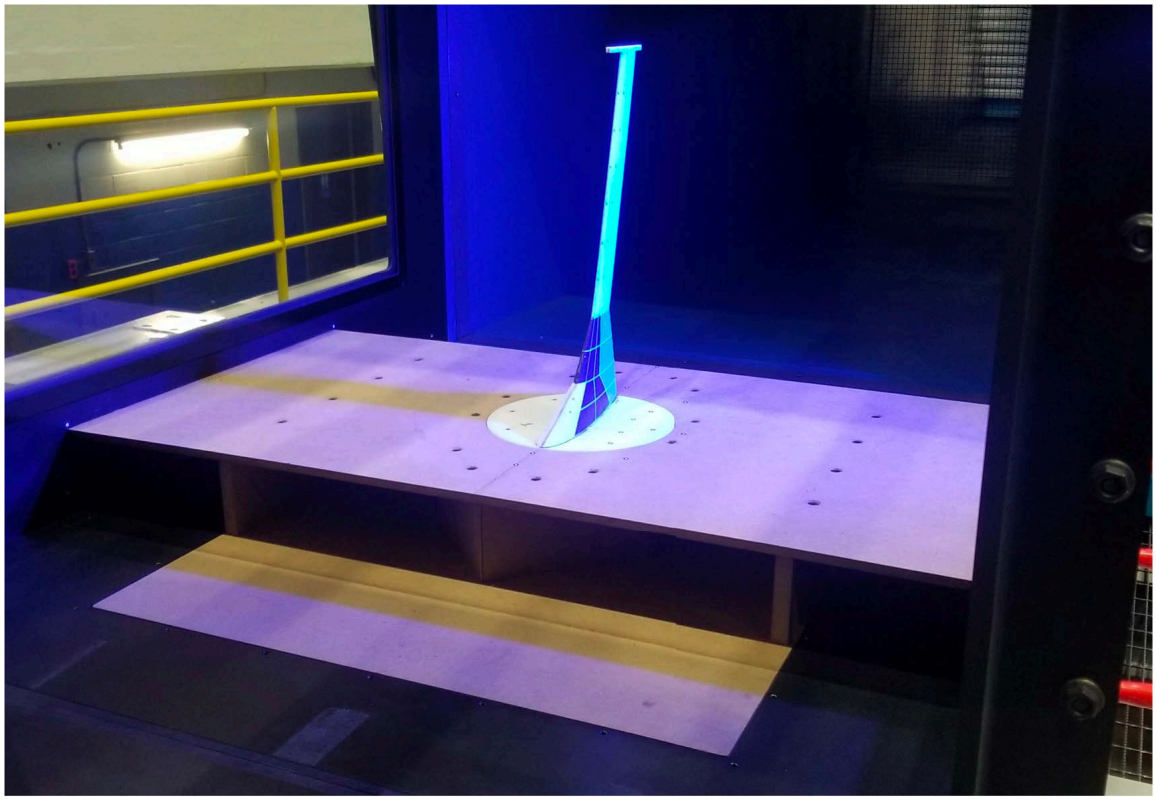

Figure 2: Wind tunnel model mounted to rotary table and splitter plate in wind tunnel

2.3 Test Article Description

A 0.48-scale static-aeroelastically scaled design of the 42 inch (1066 mm) semi-span model from Pankonien & Reich [3] resulting in a 20 inch (508 mm) semi-span model. This scaling was accomplished using the technique from Taylor et al. [10] for a 20 inch (508 mm) semi-span model was selected based on relatively low mass and high safety factor. The scale of this model was selected because it was the largest dimension achievable with in-house 3D printers. This

model is represented by the following thicknesses and material modulus seen in Figure 3.

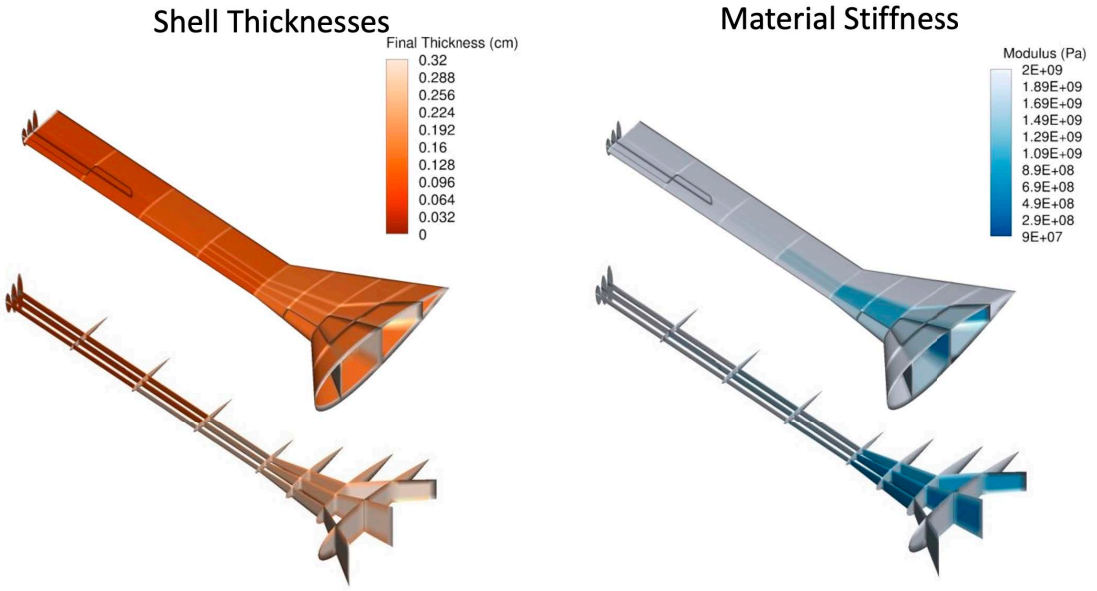

Figure 3: Thickness and material stiffness of selected design

The models were fabricated in two halves for ease of support material removal. The dividing plane was located along a plane that is parallel to the flow direction, intersecting both the leading and trailing edges of the airfoils. The variable material stiffness was realized by Polyjet multi-material printing where the digital materials selected corresponded with discrete, desired stiffnesses from the scaling optimization. The resultant material distribution can be roughly seen in Figure 4a. In this image, the darker the material corresponds with increased use of elastomer (i.e. TangoBlackPlus) and the lighter material corresponds with increased use of stiff plastic (i.e. VeroWhitePlus). The two halves of this test article cost approximately USD$700 in material to produce. However, it was noticed that the material would creep under loading over timescales longer than 10 seconds, as noted in [10].

During model fabrication, the authors became aware of a different fabrication process with similar resolution and build tray size, specifically the EOS P810 with the HT23 material, which is based on a PEKK resin with 23 percent chopped carbon fiber [12]. This process could only fabricate a single material and the material was approximately three times stiffer than the VeroWhitePlus, violating the ability to simply re-use the same geometry for an aeroelastically scaled model. However, the process was still of interest because of its similar size and resolution, and a reported material glass transition temperature of 320 degrees Fahrenheit (160 degrees Celsius). Thin structures fabricated with this material were expected to creep less at the expected wind tunnel test temperature of 72 degrees Fahrenheit (22 degrees Celsius). Accordingly the same geometry as the scaled wing was fabricated in a similar manner, resulting in two halves shown in Figure 4b. Fabricating this model cost USD$1,300.

The geometry from both of these models had a small, thin boom added to the wing tip to aid in quasi-static loading for assessing safety factor before wind tunnel testing. This boom was not expected to impact the quasi-static deflections significantly.

Finally, in the week before the wind tunnel test, the team was able to close a 0.48 geometric scale-factor, dynamically-scaled aeroelastic design. This model had a much more complex dis-

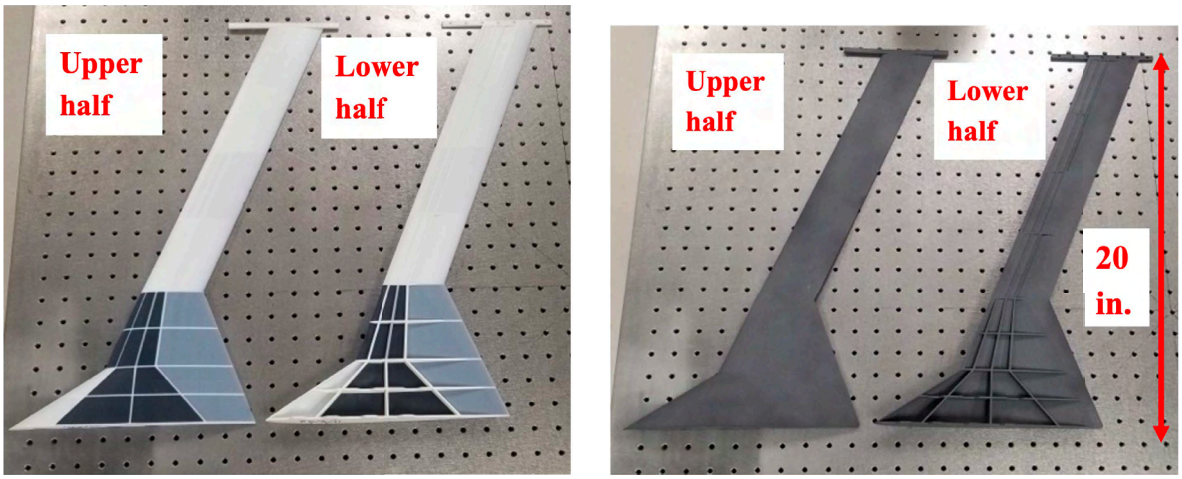

(a) Polyjet Statically Scaled Model Fabrication

(b) HT23 Model Fabrication

Figure 4: Statically-scaled test article fabrication

tribution of thicknesses and material properties, as can be seen in 5a. The optimization problem solved to achieve dynamic scaling was to match the first three natural frequencies and mode shapes of the 42 inch semi-span model from [3], subject to minimum gage thickness assessed for the printing process, and the printable materials available. Using the multi-material properties from the J750, the optimization was determined to be unable to reach a feasible solution without a small concentrated mass added to the trailing edge of the model. For the design shown here, this added mass was determined by the optimization to be 15 grams. Intuitively, this mass was needed because the full scale model had a winglet but the subscale model did not. Thus additional mass near the location of the winglet was necessary to close the design. Comparing the damping and frequency plots between the full scale and sub scale models from aeroelastic analaysis, shown in Figure 5b, the design was considered to be reasonable for testing. (Note that the frequencies in this figure have been scaled by the ratio of geometric scale factors of the wings to aid in comparison). However, due to the short timescale between the closure of the design and the test window precluding appropriate safety precautions, this mass was not included during testing.

Keeping with the goals of the test to bring multiple versions of a single design forward for aeroelastic testing, three of each static model was printed and glued together. These models were adhered to a 3D-printed adapter plate of 0.25 inch (6.35 mm) thickness using two-part epoxy with alignment controlled by a slightly-embossed outline of the root airfoil. This common adapter allowed the models to be rapidly switched during testing. An adapter plate was added to the dynamically scaled model, however only one of the dynamically scaled models was fabricated due to time constraints. Several of these models can be seen in Figure 6 prior to wind tunnel testing.

2.4 Instrumentation

Deflections of the models under differing flow conditions were measured using the non-contact technique of Digital Image Correlation (DIC), specifically, the Zeiss Aramis SRX stereo camera system. The cameras were oriented vertically to maximize resolution by aligning the aspect ratio of the image with the high aspect ratio of the models. As seen in Figure 7. Notably, the cameras were calibrated prior to the positioning of the model and viewed the model through optical glass. Manufacturer-provided stickers were attached to the model along the upper surface

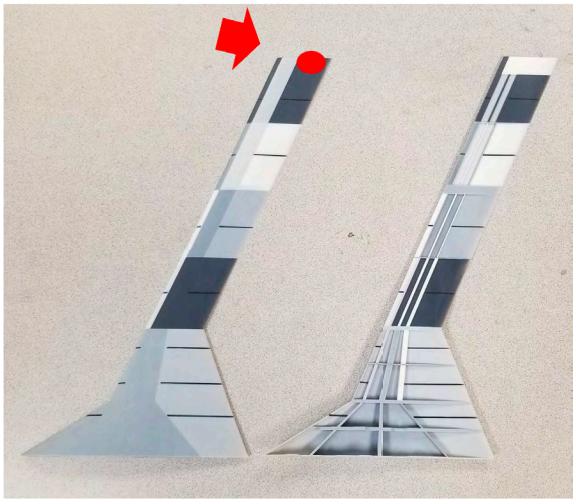

(a) Polyjet Dynamically Scaled Model Fabrication with red dot noting location of expected added 15g mass

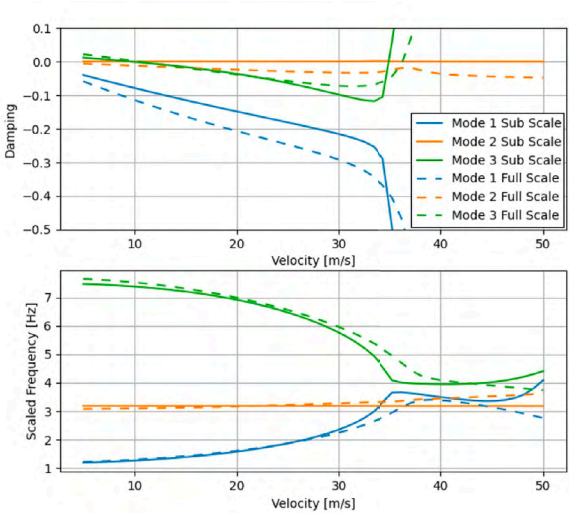

(b) Scaled Frequency and Dynamics vs Flow Velocity Plot

Figure 5: Dynamically-scaled test article fabrication

Table 1: Quasi-Static Test Matrix

Model Number	Design Description	Flow Speeds (m/s)	Angle of Attack (deg)
1	Polyjet (statically scaled)	10,20,30	0,-5.0,-2.5,0,2.5,5.0,2.5,0
2	Polyjet (statically scaled)	10,20,30	0,-5.0,-2.5,0,2.5,5.0,2.5,0
3	Polyjet (statically scaled)	10,20,30	0,-5.0,-2.5,0,2.5,5.0,2.5,0
4	HT23	10,20,30	0,-5.0,-2.5,0,2.5,5.0,2.5,0
5	HT23	10,20,30	0,-5.0,-2.5,0,2.5,5.0,2.5,0
6	HT23	10,20,30	0,-5.0,-2.5,0,2.5,5.0,2.5,0

of the wing (facing the camera). The stickers were spaced equally at 10 stations along the span, with a sticker at the leading edge, quarter chord and trailing edge of each station. These stickers allowed each model's movement in all 3 dimensions to be measured with 50 micron accuracy. For quasi-static testing the cameras acquired 5 images at rate of 1 Hz at each condition. For dynamic testing, additional lighting (not pictured) was used, and 1000 images at a rate of 200 Hz were acquired at each condition.

2.5 Static Aeroelastic Wind Tunnel Testing

For the static aeroelastic test, the primary goal was to compare the aeroelastic response of several instances of each model and their repeatability at various flow speeds. The test matrix for the six models fabricated is shown in Table 1.

A simple metric to compare the model's stiffness was created based on the displacements tracked by DIC. Since stiffness is inversely proportional to displacement for an applied load, this stiffness metric was inverted to make plotted points proportional to measured displacements, aiding interpretability.

$$Compliance = 1/K = \Delta\delta/(\Delta\alpha q S C_{L_\alpha}) \tag{2}$$

Here K is the apparent stiffness of the model, $\Delta\delta$ is the change in deflection of the model measured at a point due to change in flow conditions, $\Delta\alpha$ is the change in angle of attack of the base of the model, q is the freestream dynamic pressure, S is the surface area of the model, and C_{L_α}

Figure 6: Several aeroelastic models prior to wind tunnel testing, composed of (left two) Polyjet and (right three) HT23

is the change in lift coefficient of the airfoil due to angle of attack as determined by rigid body numerical simulations. For this study the data presented will only be for the marker at the quarter chord at the wing tip. An example of data collected for three instances of the same design is shown in 8. Here it can be seen that for a single flow condition, the repeated measurements of displacement at a single angle of attack allowed a slope to be measured that was independent of mounting error. This slope is the only measured quantity in the prior equation.

Because this metric also accounts for freestream flow speed q , the compliance of the models can be compared across test conditions, seen in Figure 9a. Since the compliance of the model should be independent of flowspeed, and increase in certainty as the flowspeed increases, the 30 m/s flowspeed should be used as the most accurate measurement for each model. It can also be seen that for all 6 models, the 10 m/s flow conditions showed the greatest error. This deviation is likely due to 10 m/s being near the lowest controllable flowspeed for the new wind tunnel. Another trend shown is that the compliance, and thus deflections, of the HT23 models are approximately 3 times lower than that of the Polyjet models, which is consistent with the approximate ratio of stiff material modulii between the two types of models.

More significantly, the HT23 models showed greater R^2 fit values across all flow speeds, as shown in Figure 9b, even eliminating the lowest flow speed conditions from consideration. This error metric comes from the fitting of the line to the displacement data, an example of which can be seen in 10a. Here the data can be shown to have hysteresis based on the direction of the angle of attack sweep. This observation along with the slow incrementation of displacement with test points shows that the Polyjet models are creeping in the wind tunnel. Neither of these

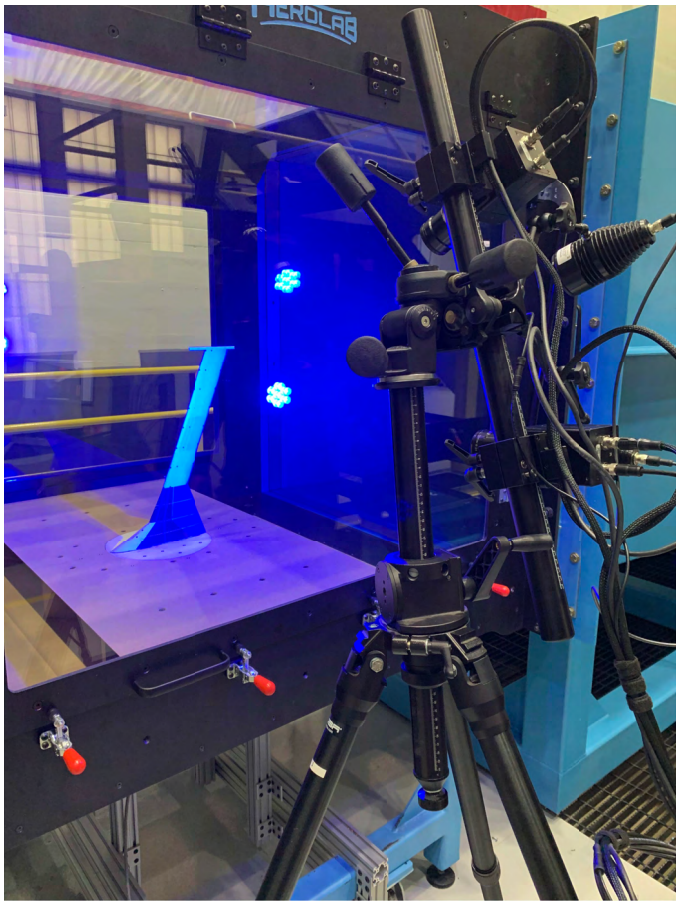

Figure 7: Tracking stickers applied to the model, measured by DIC cameras in wind tunnel

Table 2: Dynamic Test Matrix

Model Number	Design Description	Flow Speeds (m/s)	Angle of Attack (deg)
1	Polyjet (statically Scaled)	10, 20, 30	0
7	Polyjet (dynamically scaled)	11, 16, 21, 26, 31	0

effects were seen in the HT23 models, as seen in 10b. This direct observation of creep in the Polyjet models led the authors to conclude that the models produced by HT23 were preferred for quasi-static testing in future test campaigns.

2.6 Dynamic Aeroelastic Wind Tunnel Testing

Although the Polyjet models experienced creep for quasi-static test conditions, it was still part of the stretch goals of the test campaign to determine whether the 20 inch semi-span polyjet models would be usable for future dynamic tests, which could be held at low loading conditions. The test matrix for the dynamic test campaign is shown in Table 2. As can be seen, there was only one version of two different polyjet designs. The first model was a repeat of the quasi-statically scaled design from before. The second model was a new multi-material dynamically scaled design. Because the point of the test was to collect dynamic response data, and the polyjet models were known to creep, the models were kept at 0 degrees angle of attack with the flow speed incrementing slowly. No external shaker or ambient exciter was used, as it was thought that turbulence in the flow may be enough to achieve measurable frequency response.

The data in the frequency domain from the statically-scaled model can be found in Figure

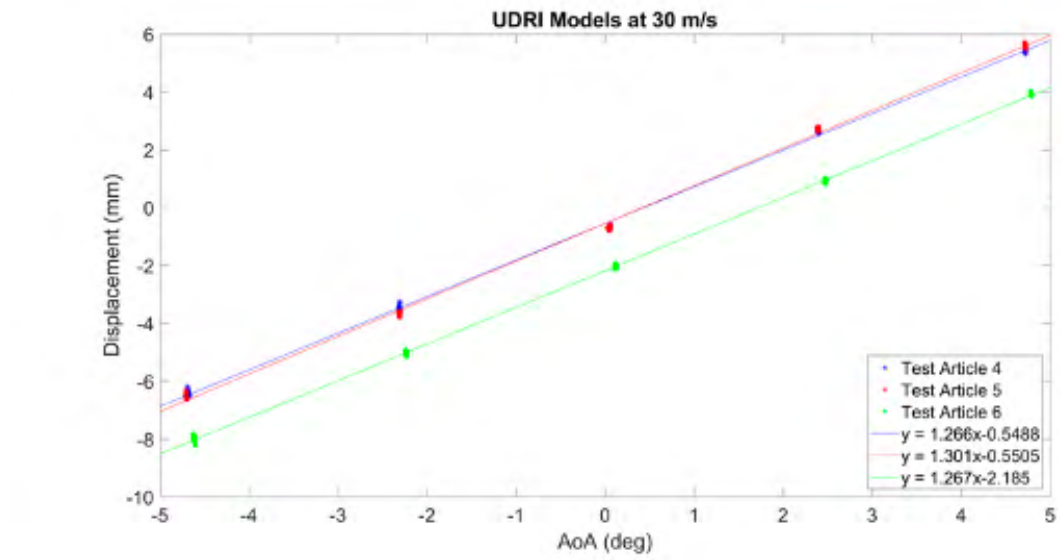

Figure 8: Extracting slope to calculate the change in displacement vs change in angle of attack

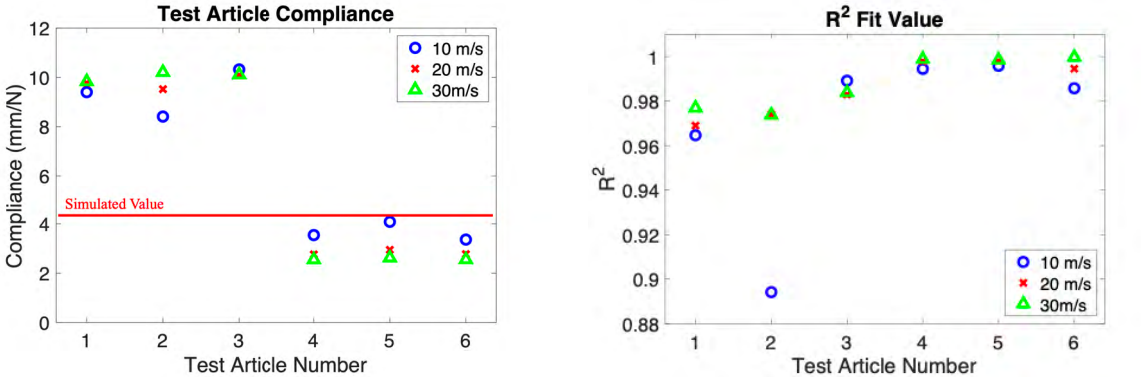

(a) Comparison of Test Article Compliance

(b) R2 Fit Value

Figure 9: Comparing test article compliance

11a. The frequency response functions show peaks where the model's modal displacement was largest due to ambient excitation at each flow speed. The red dotted lines indicate where modal analysis and prior ground vibration testing indicated there should be mode shapes. The mode shapes as expected by analysis are shown above the dotted lines. The results show fairly good agreement between the measured locations for the peaks from the test data for the first 3 modes. It should be noted however, that due to lack of anti-aliasing filter on the 200 Hz DIC data, the measurements of model frequencies above 20 Hz can be spurious.

The data for the dynamically-scaled model, shown in Figure 11b stood in stark contrast. Because of the short window prior to the wind tunnel test, no ground vibration test data was available, so only analysis data is presented. This data shows much higher damping, likely due to the increased use of elastomer in the model, as seen near the trailing edge of the root of the second model in Figure 5a. Unfortunately this added damping meant that even though there were three anticipated modes under 20 Hz, only one was observable, and it appeared to be at a higher frequency than anticipated. The measured mode was not expected to be the in-plane mode as this mode had no aeroelastic contribution.

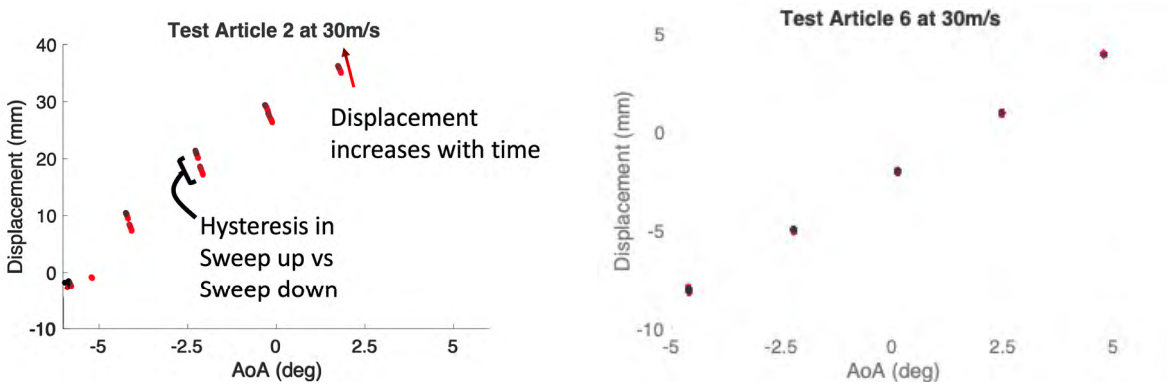

(a) Polyjet model shows creep in data

(b) HT23 Model does not show creep in data

Figure 10: Comparison of data repeatability between (left) Polyjet and (right) HT23 models

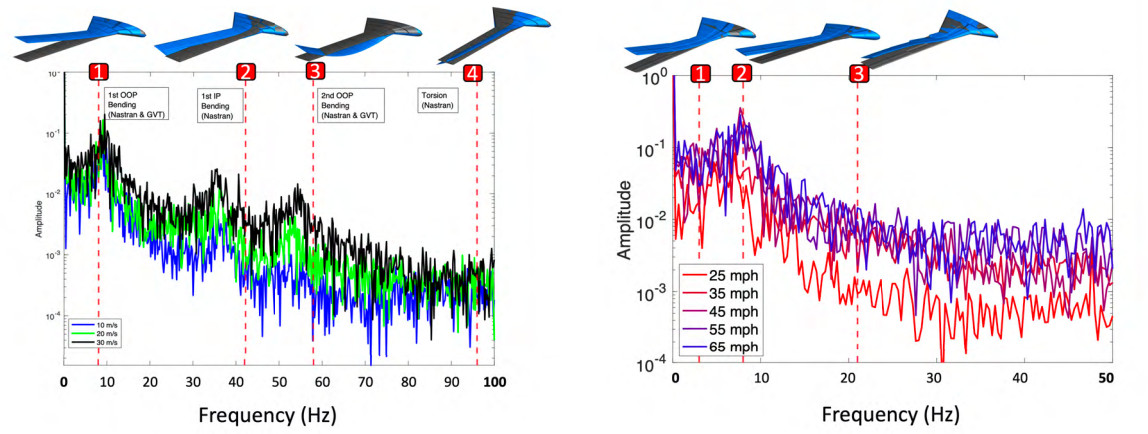

(a) Dynamic Response of Statically-Scaled Model

(b) Dynamic Response of Dynamically-Scaled Model

Figure 11: Dynamic experimental data

The combination of these results to the authors indicated that if Polyjet models are desired for the use of dynamic wind tunnel models in the new SuRF wind tunnel, additional excitation methods will be necessary due to the use of elastomer. These results also indicated to the authors that it may be desirable to use only the HT23 materials to reduce overall model damping.

3 MODEL INSPECTION

The wind tunnel models were 3D-scanned post wind tunnel test to determine the variability of the geometry for future efforts in data assimilation. The data from the scan would also be useful in explaining variability between the models. The models were scanned using the Zeiss ScanBox 5120. The scanner is capable of measuring models larger than 78.7 in (2.2 m) in size, in all 3 dimensions, with accuracy on the order of 50 microns [13]

Although this step would ideally have been completed before the wind tunnel test, due to time constraints on testing windows, the order was reversed. The Polyjet models (1-3) were not scanned because there was no way to tell how much creep was due to the testing version initial construction variability. Thus only the data for models 4-6 are presented in the following section.

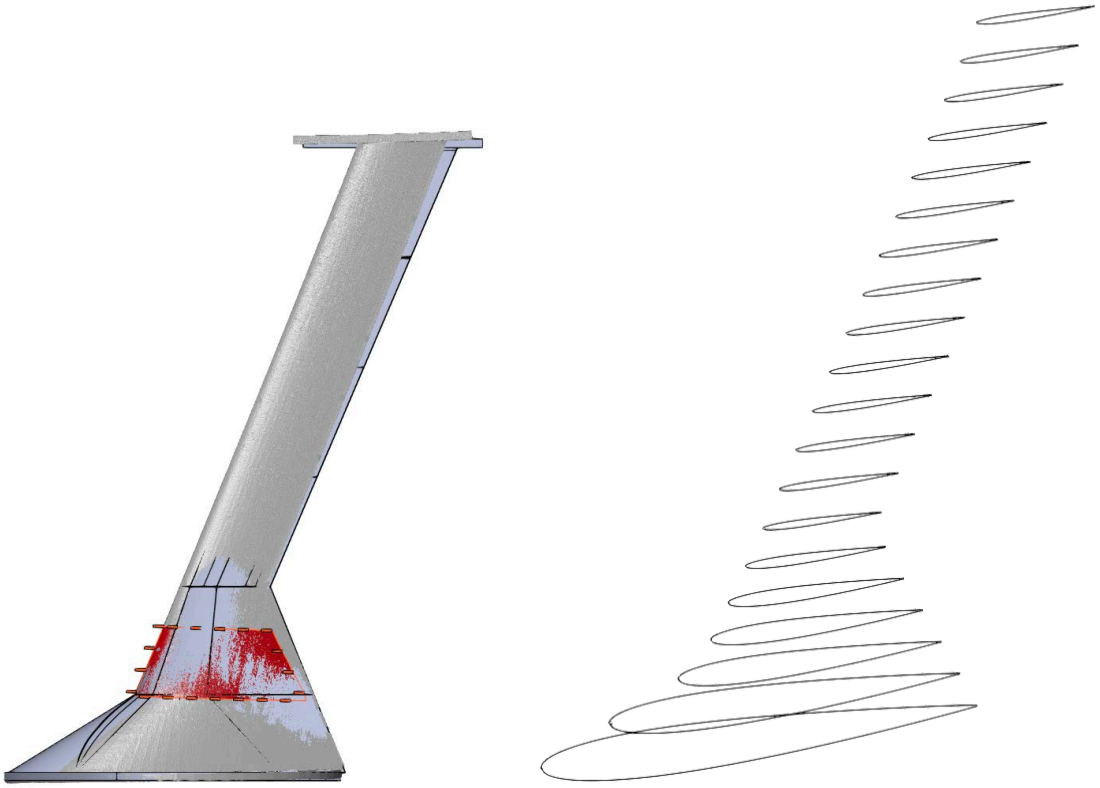

(a) Models aligned using subregion near leading edge kink

(b) Airfoils extracted from scanned data

Figure 12: Procedure for extraction airfoil data

3.1 Alignment with CAD geometry

The models were aligned with the CAD geometry by selecting a section inboard of the trailing edge crank, seen in 12a . Ideally this step would have been performed using fiducial markers on the mounting plate for each model. However, it was found that the accuracy of the DIC scan data was great enough to detect warping in the 3D-printed mounting plates, requiring a different approach. Selecting a relatively "stiff" section of the model inboard of the thin, flexible outboard section allowed for relatively small mounting deviations between the models to be rejected in favor of examining outboard deformations that could affect aeroelastic response. From "matched" geometries, airfoils could then be extracted from the scanned geometries, evenly spaced spanwise to extract more conventional aerodynamic parameters, as seen in Figure 12b.

3.2 Scan Results

The heatmaps showing deviations of the models from the as-scanned geometries can be found in Figures 13,14, and 15, with an upper and lower bound of +/- 2.54 mm. Although models 4 and 5 seem to not exhibit much twist, model 6 seems to have slight inboard negative twist with outboard positive twist. This is likely due to residual stress when adhering the upper and lower surfaces as all three models were printed in the same manner and orientation.

3.3 Resultant Twist and Camber

The typical aerodynamic parameters of twist and camber vs spanwise station were extracted from the airfoils in the scans. These values were found by algorithmically locating the leading and trailing edges of the models and comparing the airfoil values to the "root" airfoil that was

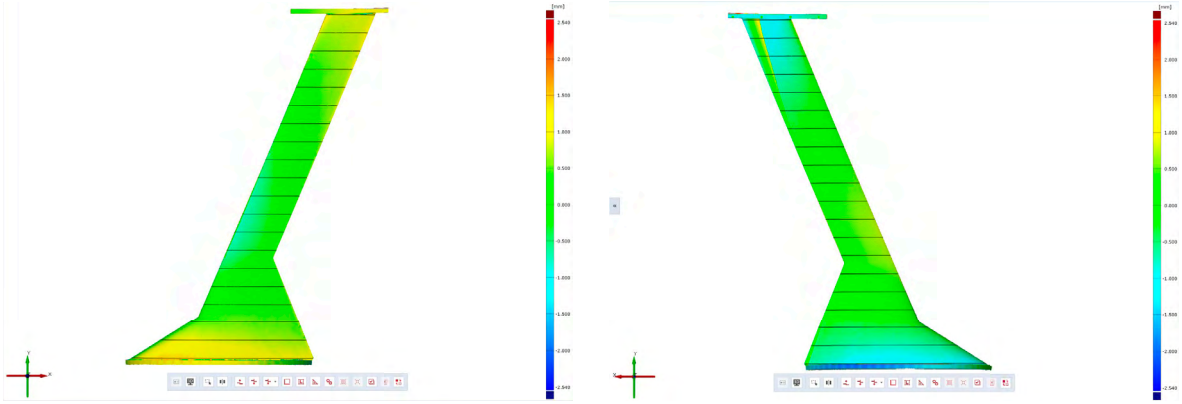

(a) Model 4, Top Surface

(b) Model 4, Bottom Surface

Figure 13: Model 4 Scans

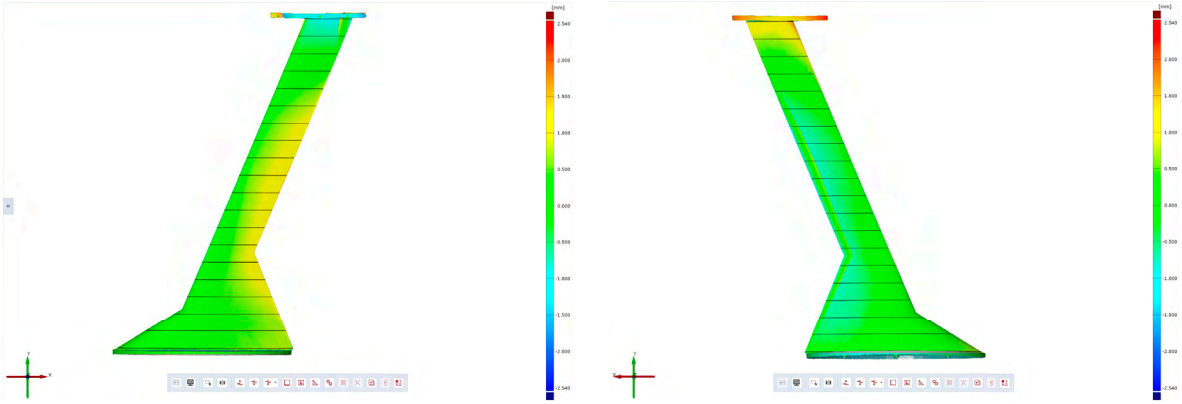

(a) Model 5, Top Surface

(b) Model 5, Bottom Surface

Figure 14: Model 5 Scans

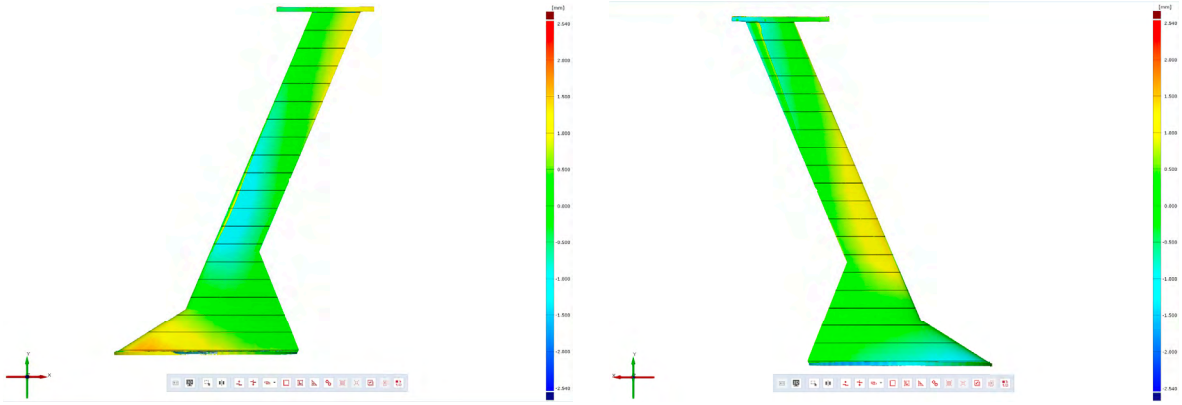

(a) Model 6, Top Surface

(b) Model 6, Bottom Surface

Figure 15: Model 6 Scans

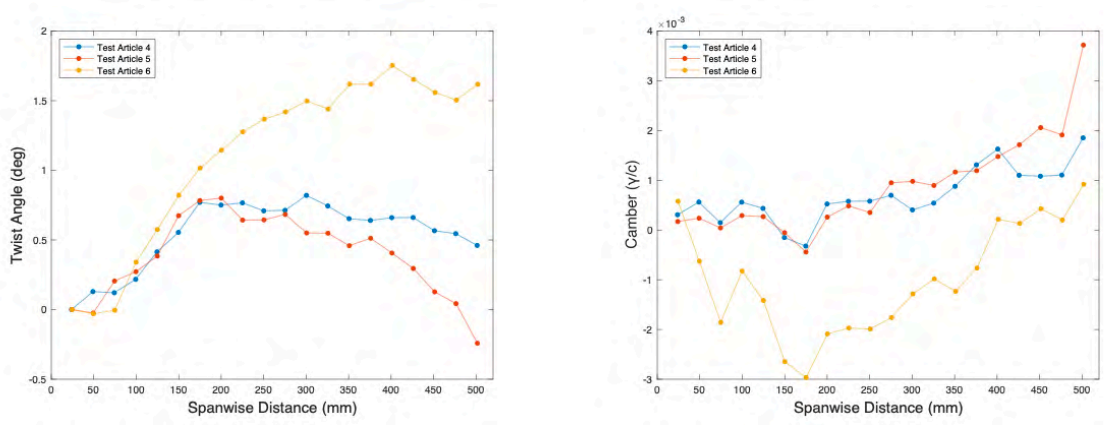

(a) Model 4-6 Twist

(b) Model 4-6 Camber

Figure 16: Model 6 Scans

located approximately 5 mm from the mounting plate. Since these models were designed with no twist or camber, any measured value can be determined to be manufacturing or measurement error. As seen in Figure 16a, models 4 and 5 exhibit less than 1 degree of twist over the span of the model, but model 6 exhibits approximately double the amount of twist outboard, reaching almost 1.75 degress. The camber for the models was much less, reaching less that 0.3% camber, even for model 6.

4 FUTURE WORK

The results shown here represent a risk reduction activity for the design, testing, and data assimilation of future aeroelastic wind tunnel models, which are expected to be up to 50% larger due to sizing and blockage considerations for the SuRF wind tunnel. Initial results for sizing a HT23 30 inch semi-span model of X-56A, performed by the authors indicate feasible designs using this technique. The lessons learned from this test are already being implemented in future test design.

5 CONCLUSIONS

The first aeroelastic test in the Subsonic Research Facility (SuRF) tunnel was performed, examining completely 3D-printed statically and dynamically scaled wind tunnel models. The scaling methodology targeted using Polyjet multi-material printing to control the model's stiffness independent of added mass. Another fabrication methodology, using a higher glass-transition temperature material, HT23, was also used. Quasi-static wind tunnel testing using Digital Image Correlation (DIC) to measure deformations due to change in angle of attack showed that the Polyjet models creeped while the HT23 models did not. Both types of models were highly repeatable between instances of the models. Dynamic wind tunnel testing was also performed using higher framerate DIC and ambient excitation from turbulence in the wind tunnel. The data showed that increasing use of elastomer in the models damped ambient vibration preventing effective measurement of relevant modes. It was then recommended that future dynamic testing use forced excitation to measure changes in aeroelastic response due to flow speed. To eliminate the effect of creep on quasi-static aeroelastic measurement it is recommended to using the HT23 material. Scans of the HT23 models show less than 1.5 degree twist and less than 0.3% camber induced by fabrication. These values are expected to be conservative upper bounds if larger models are created, as initial feasible results indicate is possible.

6 ACKNOWLEDGEMENTS

The authors greatly appreciated the support of test branches at AFRL for this work including the specific efforts of Samuel Tilmann, Ben Hagen, and Jon Geiger.

Distribution Statement A: Approved for Public Release; Distribution is Unlimited. AFRL-2024-2489.

Robert Taylor has a potential research conflict of interest due to a financial interest with Optimal Structures LLC. A management plan has been created to preserve objectivity in research in accordance with University of Texas at Arlington policy.

7 REFERENCES

[1] J. D. Bartley-Cho and J. A. Henderson, "Design and analysis of hilda/aei aeroelastic wind tunnel model," in *Collection of Technical Papers - AIAA Applied Aerodynamics Conference*, 2008.

[2] R. L. Bisplinghoff, H. Ashley, and R. L. Halfman, *Aeroelasticity*. Courier Corporation, 2013.

[3] A. M. Pankonien and G. W. Reich, "Multi-material printed wind-tunnel flutter model," *AIAA Journal*, vol. 56, no. 2, p. 793 – 807, 2018.

[4] N. Tsushima, K. Saitoh, H. Arizono, and K. Nakakita, "Structural and aeroelastic studies of wing model with metal additive manufacturing for transonic wind tunnel test by naca 0008 example," *Aerospace*, vol. 8, no. 8, 2021.

[5] B. Sharqi, C. E. Cesnik, T. Joels, and D. E. Raveh, "3d-printed swept-wing wind tunnel model characterization for aeroelastic studies," in *International Forum on Aeroelasticity and Structural Dynamics*, no. IFASD 2022-079, 2022.

[6] B. K. Stanford, "Topology optimization of low-speed aeroelastic wind tunnel models," in *AIAA Scitech 2021 Forum*, p. 1 – 9, 2021.

[7] B. K. Stanford, K. E. Jacobson, and P. Chwalowski, "Ongoing aeroelastic prediction and validation activities at nasa langley research center," in *AIAA Science and Technology Forum and Exposition, AIAA SciTech Forum 2022*, 2022.

[8] R. Fernandes, B. Hu, Z. Wang, Z. Zhang, and A. Y. Tamijani, "Analysis of additively manufactured flexible wing model," *Rapid Prototyping Journal*, vol. 30, no. 1, p. 73 – 84, 2024.

[9] J. Deslich and A. M. Pankonien, "Aeroelastically scaled rapid prototyped wind tunnel models for experimental aeroelastic testing," in *International Forum on Aeroelasticity and Structural Dynamics*, 2022.

[10] R. M. Taylor, B. Niakin, J. Deslich, Z. McFarlane, and A. M. Pankonien, "Optimization driven stiffness scaling and experimental validation of printed polymeric aeroelastic models," in *AIAA Scitech*, 2021.

[11] "Afrl's aerospace systems directorate opens new subsonic wind tunnel facility," 2021. url https://www.afrl.af.mil/News/Article/2872408/afrls-aerospace-systems-directorate-opens-new-subsonic-wind-tunnel-facility/.

[12] *HT-23*. Available at https://www.advancedlasermaterials.com/wp-content/uploads/2023/01/HT-23-Data-Sheet-2022.pdf.

[13] *ATOS ScanBox Optical 3D Coordinate Measuring Machine*. Available at https://www.capture3d.com/.../ATOS/ScanBox/2019/Brochure.pdf.